BIOCHEMISTRY
including biophysical chemistry & molecular biology
Article

Biochemistry **2011,** *50,* 25–36 25
DOI: 10.1021/bi101426s

Modifications to Surfactant Protein B Structure and Lipid Interactions under Respiratory Distress Conditions: Consequences of Tryptophan Oxidation†

Muzaddid Sarker,‡ Jarratt Rose,§ Mark McDonald,‡ Michael R. Morrow,‡ and Valerie Booth*,‡,§

‡*Department of Physics and Physical Oceanography and* §*Department of Biochemistry, Memorial University of Newfoundland, St. John's, NL, Canada*

Received September 3, 2010; Revised Manuscript Received December 3, 2010

ABSTRACT: These studies detail the altered structure−function relationships caused by oxidation of surfactant protein B (SP-B), a mode of damage thought to be important in acute respiratory distress syndrome (ARDS), a common and frequently fatal condition. An 18-residue fragment comprising the N-terminal helix of SP-B was investigated in oxidized and unmodified forms by solution and solid-state nuclear magnetic resonance (NMR), circular dichroism (CD), and molecular dynamics (MD) simulation. Taken together, the results indicate that tryptophan oxidation causes substantial disruptions in helical structure and lipid interactions. The structural modifications induced by tryptophan oxidation were severe, with a reduction in helical extent from approximately three helical turns to, at most, one turn, and were observed in a variety of solvent environments, including sodium dodecyl sulfate (SDS) micelles, dodecyl phosphocholine (DPC) micelles, and a 40% hexafluoro-2-propanol (HFIP) aqueous solution. The unmodified peptide takes on an orientation within lipid bilayers that is tilted approximately 30° away from an in-plane position. Tryptophan oxidation causes significant modifications to the peptide−lipid interactions, and the peptide likely shifts to a more in-plane orientation within the lipids. Interestingly, the character of the disruptions to peptide−lipid interactions caused by tryptophan oxidation was highly dependent on the charge of the lipid headgroup.

Lung surfactant is a mixture of lipids and proteins that allows normal breathing by reducing the surface tension created at the air−water interface in alveoli and, additionally, provides the first line of defense against inhaled microbes in the lungs. Deficiency or inactivation of lung surfactant leads to potentially fatal respiratory disorders such as neonatal respiratory distress syndrome (NRDS)[1]) in premature newborns (*1*) and acute respiratory distress syndrome (ARDS) in adults with acute injury or illness (*2*). Surfactant protein B (SP-B) is an indispensable component of the lung surfactant system (*3*). SP-B performs such crucial roles in surfactant function that its hereditary deficiency is lethal in humans (*4*) and in knockout mice (*5*). Deactivation of SP-B by antibodies also leads to respiratory distress syndrome (RDS) in rabbit models (*6*). Although a complete mechanistic description of SP-B's crucial roles in normal respiration is still unavailable, biophysical studies suggest that SP-B functions by facilitating large-scale rearrangements of surfactant lipids and stabilizing the structures required at various stages of the breathing cycle (*7*).

Lung surfactant is directly exposed to oxidative air pollutants in the alveolar space and also exposed to endogenous reactive oxygen species (ROS) produced by leukocytes and macrophages (*8*). It is thus inherently vulnerable to oxidative damage (*9*). Surfactant oxidative modifications likely play a central role in the pathogenesis of lung diseases, such as ARDS and acute lung injury (ALI) (*10*, *11*). Oxidative modifications result in dysfunction of lung surfactant and can lead to its complete inactivation (*8*, *12*−*14*). Several studies have examined the disruptive effects of ROS on individual lipid and protein components as well as on overall alterations of surfactant biophysical activity (*14*−*20*). Perhaps the most deleterious effect is observed in ROS-induced modifications of SP-B, which appear to be a severe contributing factor in surfactant inactivation (*8*, *15*, *19*). It has been shown that the oxidation of SP-B involves modification of three amino acids: the two methionines and the single tryptophan present in the protein sequence (*21*). Studies of fusogenic, lytic, and surface tension reducing activities of SP-B-based peptides have demonstrated that the tryptophan (Trp9) is critical for optimal interface affinity of SP-B (*22*, *23*). It is therefore pertinent to characterize changes in the structure of SP-B and in its interactions with lipids, resulting from the oxidative modification of Trp9, which potentially lead to a loss of SP-B function.

Tryptophan is an amino acid that typically either contributes to the stabilization of the hydrophobic core of a water-soluble globular protein or anchors a membrane protein to a polar−apolar interface (*24*). For SP-B, structural studies of Mini-B suggest that the latter case is more likely (*25*). Mini-B, a synthetic construct comprising the N-terminus and C-terminus of SP-B's

†This research was supported by a CIHR Operating Grant to V.B. and an NSERC Discovery Grant to M.R.M.

*To whom correspondence should be addressed. Phone: (709) 864-4523. Fax: (709) 864-2422. E-mail: vbooth@mun.ca.

[1]Abbreviations: NRDS, neonatal respiratory distress syndrome; ARDS, acute respiratory distress syndrome; SP-B, surfactant protein B; RDS, respiratory distress syndrome; ALI, acute lung injury; ROS, reactive oxygen species; BLES, bovine lipid extract surfactant; SDS, sodium dodecyl sulfate; DPC, dodecylphosphocholine; NMR, nuclear magnetic resonance; CD, circular dichroism; POPC, palmitoyloleoylphosphatidylcholine; MD, molecular dynamics; DPPC, dipalmitoylphosphatidylcholine; POPG, palmitoyloleoylphosphatidylglycerol; HPLC, high-performance liquid chromatography; MALDI-TOF, matrix-assisted laser desorption ionization time-of-flight; HFIP, hexafluoro-2-propanol; DSS, 2,2-dimethyl-2-silapentane 5-sulfonate; DTT, dithiothreitol; PFG, pulsed field gradient; rmsd, root-mean-square deviation; DSSP, define secondary structure of proteins.

Published on Web 12/03/2010

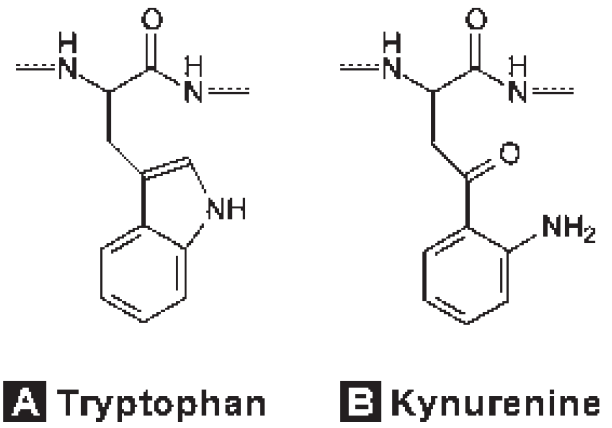

FIGURE 1: Chemical structures of tryptophan (Trp) (A) and one of its oxidized forms, kynurenine (Kyn) (B).

four predicted helices, performs as well as the full-length protein in surfactant deficient rat models and likely encompasses the key functional regions of SP-B (*26*). The high-resolution structure of Mini-B, determined in lipid-mimetic detergent micelles, shows that the side chain of Trp9 (Trp2 in Mini-B) does not appear to contribute to the interhelix hydrophobic contacts and therefore that its role is most likely to interact with the lipids to help anchor Mini-B at the lipid headgroup−acyl chain interface (*25*).

Although methionine may become oxidized more easily than tryptophan, we have focused on the oxidation of the latter, as this modification to SP-B likely contributes more severely to surfactant inactivation. Bovine lipid extract sufactant (BLES), a therapeutic form of lung surfactant, remains functional despite evidence that it contains SP-B with some degree of methionine oxidation (*21*). However, BLES treated with Fenton reagents, which induces oxidation of SP-B tryptophan, exhibits a loss of surface activity (*21*).

We have used an 18-residue N-terminal fragment of SP-B, termed SP-B_{8-25}, to assess the changes that oxidation of Trp9 may cause in the structure and/or lipid interactions of SP-B. The SP-B_{8-25} fragment contains the N-terminal α-helix of SP-B and also corresponds to the N-terminal half of Mini-B. Two variants of the peptide were used: the unmodified Trp-SP-B_{8-25} that retains tryptophan at position 2 and the oxidized Kyn-SP-B_{8-25} in which tryptophan has been replaced with one of its oxidized forms, kynurenine (Kyn) (Figure 1). The differences in the structures and lipid interactions of the two peptides have been probed in membrane-mimetic anionic sodium dodecyl sulfate (SDS) and zwitterionic dodecyl phosphocholine (DPC) micelles, using solution nuclear magnetic resonance (NMR), circular dichroism (CD), and diffusion NMR. Solid-state deuterium (^{2}H) NMR was also employed to determine the orientation and dynamics of the unmodified peptide in a palmitoyloleoylphosphatidylcholine (POPC) bilayer. Lastly, unrestrained molecular dynamics (MD) simulations of both peptides were performed in dipalmitoylphosphatidylcholine (DPPC)/palmitoyloleoylphosphatidylglycerol (POPG) monolayers to gain additional insight into the mechanisms by which oxidation affects the structure and lipid interactions of SP-B_{8-25}.

MATERIALS AND METHODS

Peptide Synthesis and Purification. Two variants of the SP-B_{8-25} peptide were synthesized and purified. The amino acid sequence, with either Trp or Kyn at position 2, was Cys-Trp/Kyn-Leu-Cys-Arg-Ala-Leu-Ile-Lys-Arg-Ile-Gln-Ala-Met-Ile-Pro-Lys-Gly. The peptides were produced by solid-phase chemical synthesis employing *O*-fluorenylmethoxycarbonyl (Fmoc) chemistry, on a CS336X peptide synthesizer (C S Bio Co., Menlo Park, CA) following the manufacturer's instructions. The peptides were synthesized at a 0.2 mmol scale with a single coupling, using prederivatized Rink amide resin. Resin and all Fmoc amino acids were purchased from C S Bio Co., with the exception of Fmoc kynurenine, which was purchased from Advanced ChemTech (Louisville, KY). Organic solvents and other reagents used for the synthesis and purification were high-performance liquid chromatography (HPLC) grade or better and purchased from Fisher Scientific (Ottawa, ON) and Aldrich Chemical (St. Louis, MO). Deprotection and cleavage of the peptides from the resin were conducted with a trifluoroacetic acid (TFA)/water (95:5 by volume) cleavage cocktail followed by cold precipitation with *tert*-butyl ether. The crude products were purified by preparative reverse-phase HPLC in a Vydac C-8 column by use of a water/acetonitrile linear gradient with 0.1% TFA as the ion pairing agent. The molecular weights of the peptides were confirmed by matrix-assisted laser desorption ionization time-of-flight (MALDI-TOF) mass spectrometry. The purified peptides were lyophilized and stored at 4 °C. A second sample of Trp-SP-B_{8-25} was synthesized for ^{2}H NMR studies and contained deuterated methyl groups in the alanine residues at positions 6 and 13. Ala6 was 100% labeled, while Ala13 was only 50% labeled so we could distinguish between the two labels in the ^{2}H NMR spectra.

NMR Sample Preparation. Solution NMR samples of both Trp-SP-B_{8-25} and Kyn-SP-B_{8-25} were prepared using three different solvent systems: SDS micelles, DPC micelles, and 40% hexafluoro-2-propanol (HFIP). All samples contained 1 mM peptide, 0.4 mM 2,2-dimethyl-2-silapentane 5-sulfonate (DSS), 0.2 mM NaN_3, 1 mM freshly prepared dithiothreitol (DTT), and 10% D_2O. Additionally, the micelle samples contained 100 mM SDS or DPC (98% deuterated; Cambridge Isotopes, Andover, MA) and 90% H_2O, and the HFIP samples contained 40% HFIP (98% deuterated; Cambridge Isotopes) and 50% H_2O. The samples were set to pH 7.0 using NaOH and HCl, without taking the isotope effects into account. Oriented ^{2}H NMR samples were prepared by depositing a Trp-SP-B_{8-25}/POPC (Avanti Polar Lipids, Alabaster, AL) mixture (3.5%, w/w), dissolved in a chloroform/methanol mixture (1:1 v/v), onto stacked mica plates as described elsewhere (*27*). Samples were dried under vacuum and hydrated (95% humidity) to establish uniformly oriented lipid bilayers.

Collection and Processing of Solution NMR Data. A set of one-dimensional (1D) ^{1}H, two-dimensional (2D) ^{1}H−^{1}H TOCSY, and 2D ^{1}H−^{1}H NOESY experiments was performed for each solution SP-B_{8-25} sample on a Bruker (Billerica, MA) Avance II 14.1 T (600 MHz) spectrometer equipped with z-gradients and an inverse triple-resonance TXI probe. The NMR data were collected and processed using Bruker Topspin version 2.0. The pulse length (P_1) and the transmitter offset (O_1) were optimized for each sample before the full set of NMR experiments was run. The NMR spectra were recorded at 37 °C to match the physiological temperature. The experiments used the water-gate water suppression technique (*28*). For 1D ^{1}H experiments, data were collected with 32 scans and processed using an exponential apodization function with 1 Hz line broadening. The 2D ^{1}H−^{1}H TOCSY experiments were performed with a 60 ms mixing time and either 80 or 128 scans. A total of 2048

and 512 data points were collected in the F_2 and F_1 dimensions, respectively, and the processed spectra had 1024 points in both dimensions. The 2D ^{1}H−^{1}H NOESY experiments were performed with a 200 ms mixing time and 128 scans. A total of 2048 and 512 data points were collected in the F_2 and F_1 dimensions, respectively, and the processed spectra had 1024 points in both dimensions. All TOCSY and NOESY spectra were processed using the Qsine apodization function with a sine bell shift of 2.

Collection and Processing of Diffusion NMR Data. Diffusion-ordered spectroscopy (DOSY) experiments were performed for the micelle samples on the same Bruker Avance II 14.1 T (600 MHz) spectrometer employing pulsed field gradient (PFG) NMR (*29*). The pulse sequence used a stimulated echo with bipolar gradient pulses and one spoil gradient (*30*), followed by a 3-9-19 pulse for water suppression (*31*). The pseudo-2D DOSY spectra were produced using Bruker Topspin version 2.0. The translational diffusion coefficients were derived from the underlying 1D ^{1}H experiments using the equation for the attenuation of signal

$$\ln[S(k)/S(0)] = -D_C k$$

$$\text{with } k = \gamma^2 g^2 \delta^2 (\Delta - \delta/3)$$

where $S(k)$ is the observed signal intensity, $S(0)$ is the unattenuated signal intensity, D_C is the diffusion coefficient, γ is the gyromagnetic ratio of the observed nucleus (^{1}H), g is the gradient strength, δ is the gradient pulse length, and Δ is the diffusion time. The diffusion time was kept constant at 100 ms. The gradient pulse length was optimized for each sample and set between 4 and 6 ms. The maximum amplitude of the gradient strength was 35 G/cm. The ^{1}H signals were attenuated to ~5% of their initial amplitudes with an increase in gradient strength from ~2 to ~95% in 32 steps. Experiments were performed at 37 °C for SDS samples, but at 25 °C for DPC samples to minimize the effect of thermal convection. The integrated signal intensities were exported into Igor Pro for curve fitting. The diffusion coefficient was determined from the slope of the linear fit of $\ln[S(k)/S(0)]$ versus k. The observed diffusion coefficient was converted into the apparent hydrodynamic diameter, using the Stokes−Einstein equation

$$D_C = k_B T/3\pi\eta d_{HA}$$

where k_B is the Boltzmann constant, T is the absolute temperature, η is the viscosity of the solution, and d_{HA} is the apparent hydrodynamic diameter of the particle. The viscosity of pure water, 6.92×10^{-4} kg m^{-1} s^{-1} at 37 °C and 8.91×10^{-4} kg m^{-1} s^{-1} at 25 °C, was used for the viscosity of the solution.

Collection and Processing of Solid-State ^{2}H NMR Data. ^{2}H NMR spectra were recorded at 61 MHz (9.4 T) using an in-house assembled spectrometer and probe. Spectra were recorded using a quadrupole echo pulse sequence (*32*) with phase cycling and $\pi/2$ pulses with a duration of 7 μs separated by 35 μs. Data were collected using a 1 μs dwell time and 8192 points. Oversampling by a factor of 4 was applied to give an effective dwell time of 4 μs, and the data were left-shifted to place the echo maximum at the first point in the free induction decay (*33*). Spectra were obtained by signal averaging over 200000 transients with a repetition time of 900 ms, using an in-house constructed flat transceiver coil (dimensions of 15 mm × 15 mm × 3 mm). Data were smoothed with a 200 Hz line broadening filter. Coil orientation was adjusted so that the lipid bilayer normal was either parallel or perpendicular to the spectrometer magnetic field. All spectra were recorded at 25 °C. The orientation dependence of the ^{2}H quadrupole echo was used to determine the time- and ensemble-averaged orientation of the peptide in the lipid bilayer, assuming an α-helical geometry for Trp-SP-B$_{8-25}$. The peptide orientation was defined by two coordinates, the tilt angle, τ, that the helix axis makes with the lipid bilayer normal and the azimuthal angle, ρ, that defines the orientation, relative to a reference direction, of a radial line from the helix axis to the C_α atom of a reference residue in a plane perpendicular to the helix axis, here taken to be Ala6. The reference direction ($\rho = 0°$) points in a direction that is simultaneously perpendicular to the helix axis and coplanar with the bilayer normal and the helix axis (*34*, *35*). Probable sets of τ and ρ were identified via a multidimensional grid search for minima in the root-mean-square deviation (rmsd) between the observed and calculated splittings (*34*, *35*).

Collection and Processing of CD Data. CD spectra, in the far-ultraviolet (far-UV) region (from 260 to 190 nm), were recorded for all Trp- and Kyn-SP-B$_{8-25}$ solution samples using a Jasco (Easton, MD) 810 spectrapolarimeter. The CD data were acquired at 37 °C using a quartz cuvette with a path length of 0.1 mm. The solution NMR samples were transferred to the cuvette without changing the sample conditions. The temperature was controlled by a CTC-345 circulating water bath. The scanning speed of the instrument was set at 100 nm/min with normal sensitivity. Five accumulations were collected for each sample in 0.1 nm steps. The molar ellipticity $[\theta]$ was calculated using the equation suggested in ref *36*.

$$[\theta] = \theta_{obs}/(10LC)$$

where θ_{obs} is the observed ellipticity, L is the path length of the cell (0.01 cm), and C is the number of amino acids multiplied by the molar concentration of the peptide (0.018 M). The concentration was determined from the weight of the dry peptide used to prepare the samples. The secondary structural content was calculated from the molar ellipticity data using the method described in ref *37*.

Molecular Dynamics Simulation. Unrestrained 50 ns MD simulations were run with both Trp-SP-B$_{8-25}$ and Kyn-SP-B$_{8-25}$ in 7:3 DPPC/POPG monolayers using GROMACS (*38*). DPPC and POPG were chosen as they are the most abundant surfactant phospholipids with zwitterionic and anionic headgroups, respectively. The 7:3 ratio was chosen as this is commonly employed in studies of model lung surfactant and roughly approximates the amount of anionic lipid, as well as the amount of unsaturated lipid. The monolayers were prepared with an area per lipid of 60 nm^2/molecule following the procedures described elsewhere (*39*). The starting structure of Trp-SP-B$_{8-25}$ was taken from the corresponding fragment of Mini-B in SDS (*25*). The starting structure of Kyn-SP-B$_{8-25}$ was prepared via replacement of the tryptophan of SP-B$_{8-25}$ with a kynurenine. Kynurenine's structure and topology parameters were derived from Gaussian calculations (*40*) that utilized a Hartree−Fock/6-31G(D) level of theory to obtain GROMACS compatible parameters for this nonstandard residue. The peptide was placed in an elliptical hole in the monolayer; Tip4p water was added to the polar side of the monolayer, and the appropriate number of water molecules were replaced with sodium counterions to neutralize the charge of the system. The final system had 73 DPPC molecules, 30 POPG molecules, one peptide, and 7976 water molecules. Energy minimization was applied to the system, and then a 10 ps

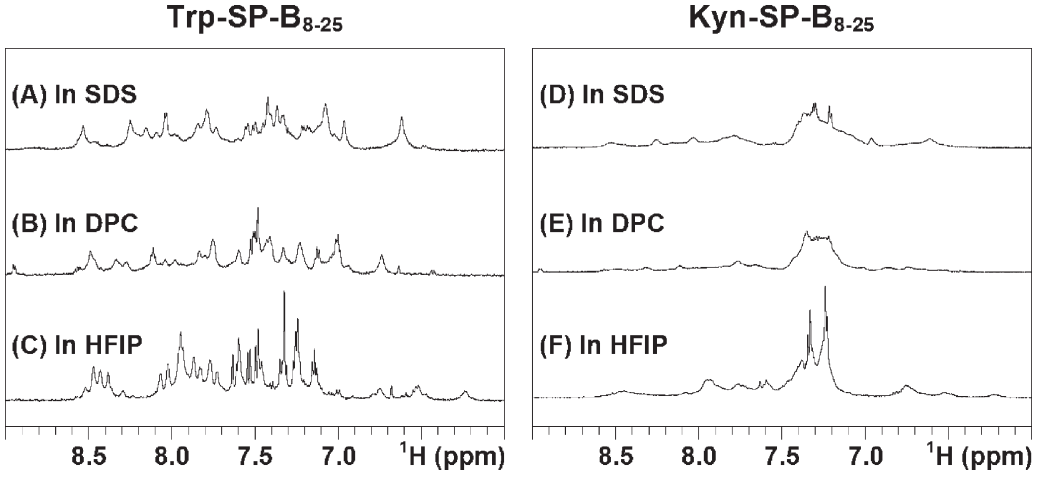

FIGURE 2: HN regions (6−9 ppm) of the 1D ^{1}H spectra of Trp-SP-B_{8-25} and Kyn-SP-B_{8-25} in various environments. The left panel shows the spectra of 1 mM Trp-SP-B_{8-25} in 100 mM SDS (A), 100 mM DPC (B), and 40% HFIP (C). The right panel shows the spectra of 1 mM Kyn-SP-B_{8-25} in 100 mM SDS (D), 100 mM DPC (E), and 40% HFIP (F). All spectra in each panel are shown with the same intensity scale, but the intensity (height) of the right panel is reduced by half with respect to the left panel.

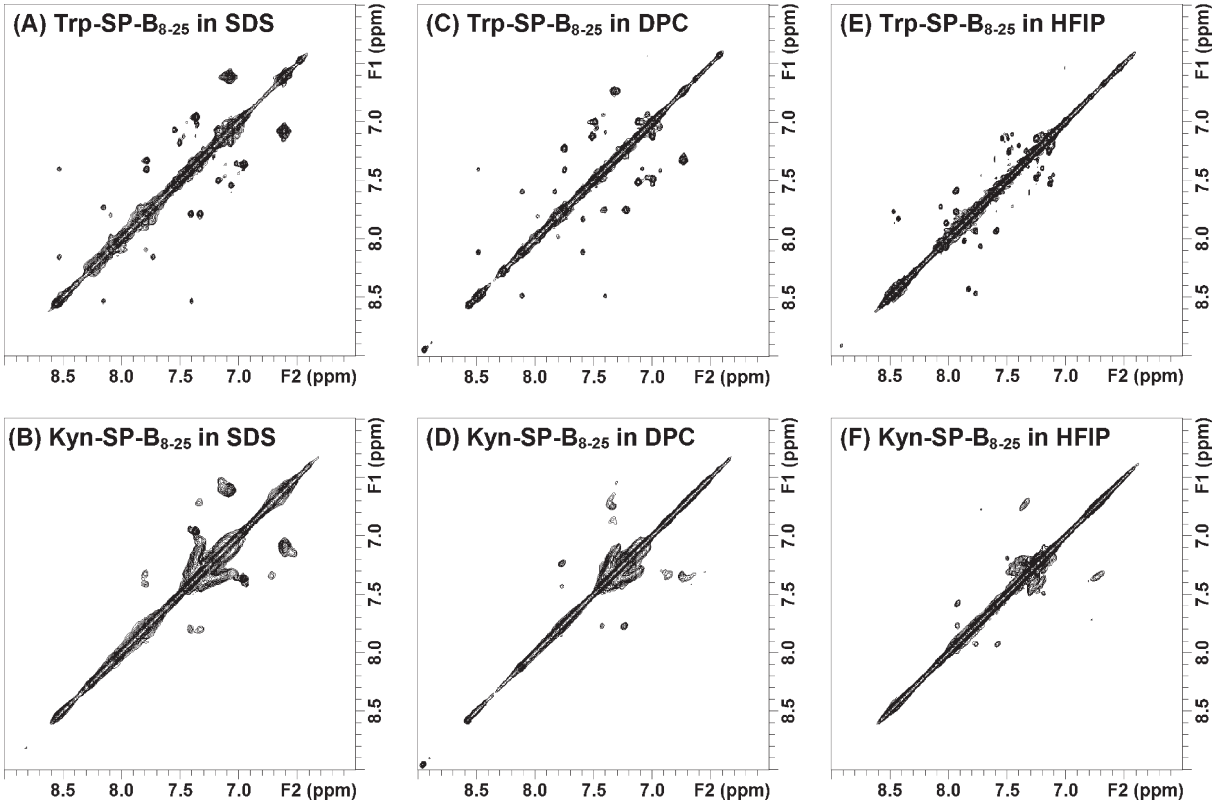

FIGURE 3: HN−HN regions (6−9 ppm) of the 2D ^{1}H−^{1}H NOESY spectra of Trp-SP-B_{8-25} and Kyn-SP-B_{8-25} in various environments. Left panels show the HN−HN correlations for 1 mM Trp-SP-B_{8-25} (A) and 1 mM Kyn-SP-B_{8-25} (B) in 100 mM SDS. Middle panels show the HN−HN correlations for 1 mM Trp-SP-B_{8-25} (C) and 1 mM Kyn-SP-B_{8-25} (D) in 100 mM DPC. Right panels show the HN−HN correlations for 1 mM Trp-SP-B_{8-25} (E) and 1 mM Kyn-SP-B_{8-25} (F) in 40% HFIP. All spectra are shown with the same contour level (intensity scale).

simulation was run with position restraints on the peptide and lipids. The force field employed was based on optimized potential for liquid systems: all atoms (OPLS-AA) (*41*) with lipid topology files from ref *42*. The production runs were 50 ns unrestrained MD simulations with the temperature maintained at 310 K using Berendsen temperature coupling and a constant box size (i.e., NVT).

RESULTS

A set of 1D ^{1}H, 2D ^{1}H−^{1}H TOCSY, and 2D ^{1}H−^{1}H NOESY solution NMR spectra was acquired for each of the Trp-SP-B_{8-25} and Kyn-SP-B_{8-25} samples in anionic SDS micelles, zwitterionic DPC micelles, and 40% HFIP. An indication of the relative degree of structuring of the peptides can be obtained via comparison of the dispersion of signals in the amide proton (HN) regions (6−9 ppm) of the 1D ^{1}H spectra (Figure 2), as well as in the HA-HN regions of the 2D spectra (not shown). In both SDS and DPC micelles, as well as in 40% HFIP, the signals of Trp-SP-B_{8-25} are well-dispersed, indicating that the peptide is structured under these conditions. On the other hand, the spectra of Kyn-SP-B_{8-25} look quite different. In spite of a few intense signals in the 7.1−7.5 ppm region, distinct and dispersed backbone

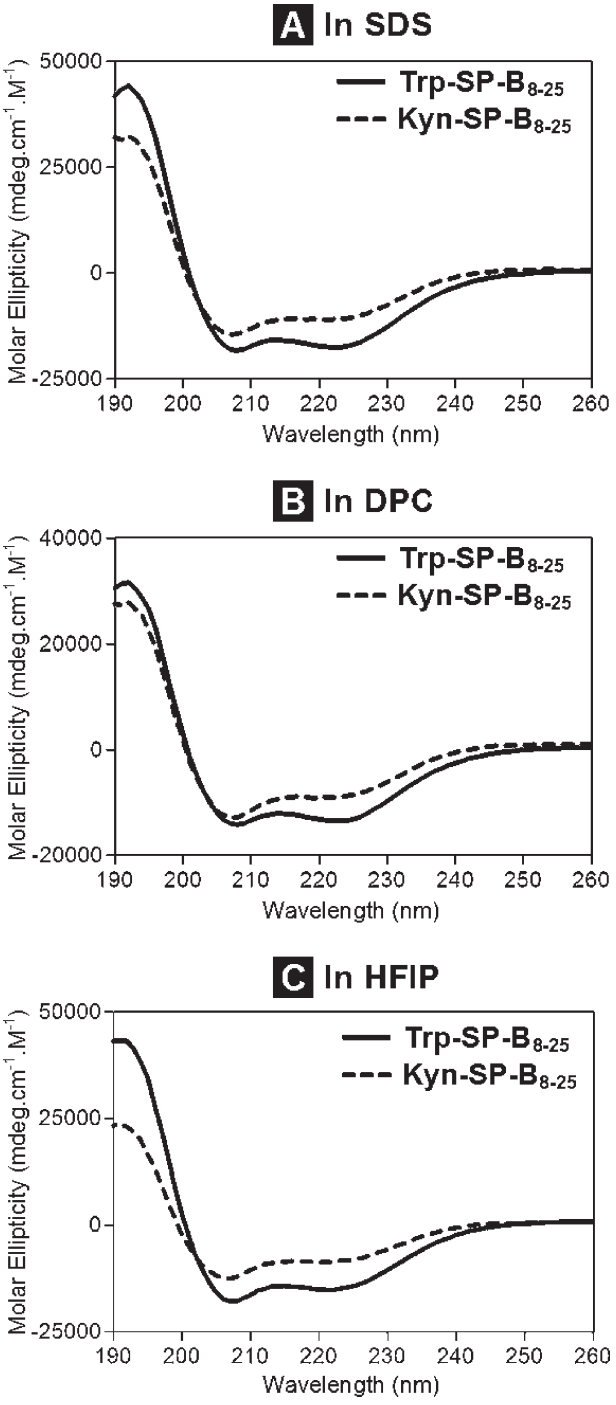

FIGURE 4: Far-UV CD spectra of 1 mM Trp-SP-B_{8-25} and 1 mM Kyn-SP-B_{8-25} in 100 mM SDS (A), 100 mM DPC (B), and 40% HFIP (C).

HN peaks are not visible. The oxidized peptide thus appears much less structured than the unmodified peptide.

The length of the helix in each sample can be estimated from the number of intense backbone HN−HN correlations present in the 2D NOESY spectra (*43*). Trp-SP-B_{8-25} displays seven to nine such correlations in both micelles and organic solvent environments (Figure 3), indicating an α-helix 8−10 amino acids in length, i.e., containing approximately three helical turns. However, the spectra of Kyn-SP-B_{8-25} in these same environments exhibit only approximately two strong HN−HN correlations (Figure 3), corresponding to only approximately three amino acids adopting the helical conformation, i.e., at most one helical turn.

Table 1: Helix Content of Trp-SP-B_{8-25} and Kyn-SP-B_{8-25} in Various Environments, Calculated from the Molar Ellipticities Obtained from the CD Spectra (Figure 5) following the Method Described in ref *37*

	SDS	DPC	HFIP
Trp-SP-B_{8-25}	52%	38%	41%
Kyn-SP-B_{8-25}	27%	20%	19%
difference	−25%	−18%	−22%

To confirm that the drastic reduction in the level of peak dispersion and the number of peaks in solution NMR spectra for Kyn-SP-B_{8-25}, when compared to those of Trp-SP-B_{8-25}, did not result from aggregation of the oxidized peptide, we performed SDS−PAGE for both peptides under all three conditions. For the SDS and HFIP samples, Trp-SP-B_{8-25} and Kyn-SP-B_{8-25} ran at exactly the same molecular mass, indicating no differences in aggregation properties (data not shown). The DPC samples could not be clearly visualized on the gel presumably because of charge interactions between the SDS and DPC.

To complement the solution NMR data, we recorded circular dichroism spectra for all SP-B_{8-25} samples. Like the NMR data, the CD data also indicate that replacement of tryptophan with kynurenine leads to a substantial reduction in the fraction of the peptide that is helically structured, under both micelle and organic solvent conditions (Figure 4 and Table 1). In SDS, 52% of Trp-SP-B_{8-25} but only 27% of Kyn-SP-B_{8-25} is helical, i.e., a reduction of 25% in helical content. Similarly, the helix content is reduced by 18% in DPC (from 38% for Trp-SP-B_{8-25} to 20% for Kyn-SP-B_{8-25}) and by 22% in HFIP (from 41% for Trp-SP-B_{8-25} to 19% for Kyn-SP-B_{8-25}). In all three environments, a concomitant increase in the random coil percentage occurs: 18% for SDS, 13% for DPC, and 15% for HFIP.

A solid-state ^{2}H NMR study was performed using the alanine-deuterated version of the peptide to gain insight into the orientation and dynamics of Trp-SP-B_{8-25} in a POPC bilayer environment. From the ^{2}H quadrupolar doublet splittings (Figure 5A), a minimum in the rmsd between calculated and experimental splittings provides a solution for the peptide orientation with a tilt angle τ of 62° and azimuthal angle ρ of 193° (Figure 5B). This is the only solution in the (τ,ρ) = (0−180°,180−360°) quadrant, although because of the symmetry of the bilayer, there are equivalent solutions in the other three quadrants [(τ,ρ) = (118°,13°), (298°,13°), and (242°,193°)]. It is known from the high-resolution structure of Mini-B (*25*) that the positions of both ^{2}H-labeled residues (Ala6 and Ala13) and positively charged residues (Arg5, Lys9, and Arg10) are on the same face of the peptide. A ρ of 193° indicates that the hydrophilic face of the peptide is predominantly aligned with the plane of the lipid bilayer and therefore in contact with the zwitterionic lipid headgroups (Figure 5C). A τ of 62 ± ∼10° (defined with respect to the bilayer normal) indicates that the axis of the unmodified SP-B_{8-25} helix has a substantial tilt, of ∼30°, away from a purely in-plane position in the bilayer (Figure 5D). While it is known that for helices with near-transmembrane orientation peptide dynamics can lead to underestimations of tilt angle, for peptides that are in-plane or near in-plane, peptide dynamics are not expected to affect the calculation of the tilt angle in a significant way (*44*). Also, the well-resolved ^{2}H quadrupolar line splittings obtained for the perpendicular placement of the sample in the spectrometer magnetic field indicate that the peptide is rapidly reorienting about the bilayer

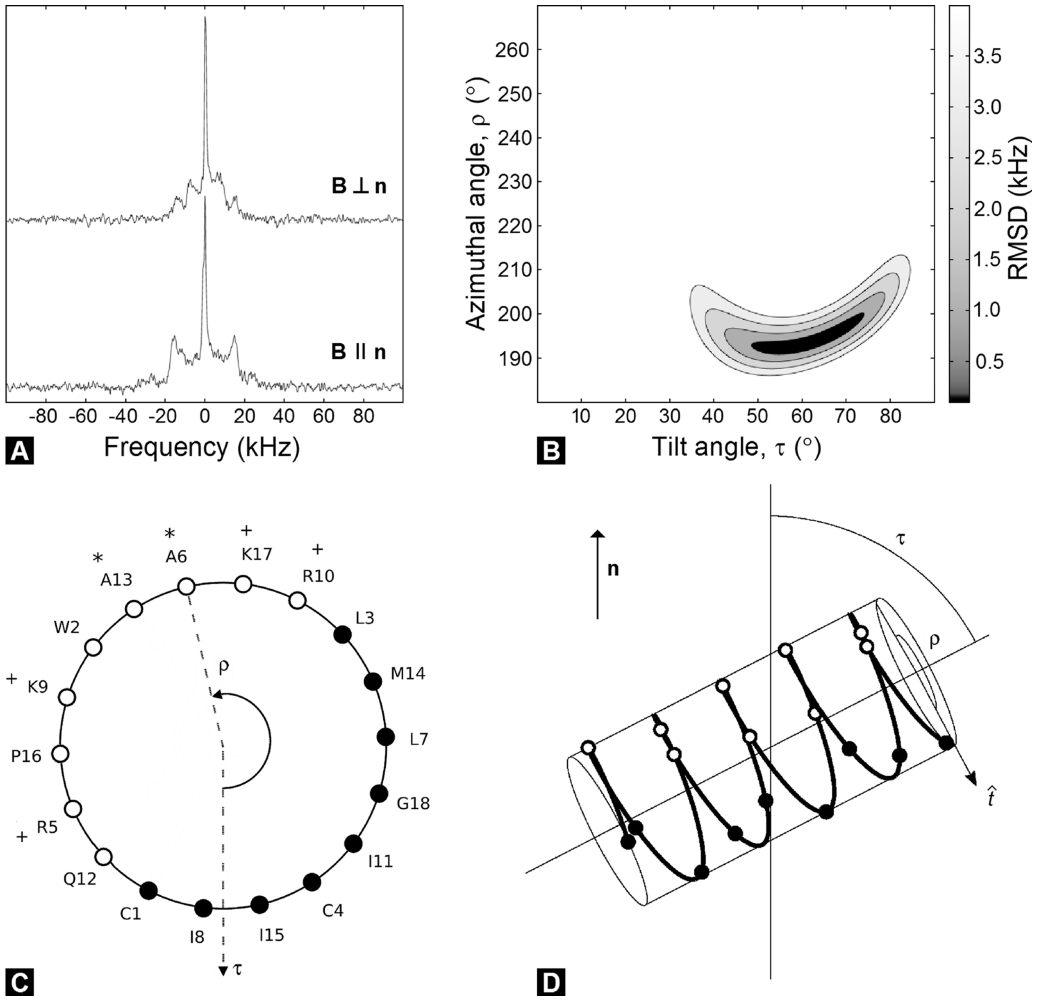

FIGURE 5: Orientation of unmodified SP-B_{8-25} in POPC bilayers as revealed by solid-state ^{2}H NMR. (A) ^{2}H NMR spectra of the peptide with deuterated alanines (Ala6 and Ala13) in oriented lipid bilayers. In the top spectrum, the lipid bilayer normal (n) is oriented perpendicular to the spectrometer magnetic field B. In the bottom spectrum, the lipid bilayer normal is oriented parallel to the spectrometer magnetic field. (B) Contour plot of the rmsd from all possible splittings as a function of tilt angle, τ (0−90° in 0.1° increments), and azimuthal angle, ρ (180−270° in 0.1° increments). The optimal solution for τ (62°) and ρ (193°) for Ala6 is indicated by the contour minima. (C) Helical wheel showing the peptide orientation (τ = 62°, and ρ = 193°) as a projection down the helical long axis (from N- to C-terminus into the page). Charged (Arg and Lys) and deuterated (Ala) residues are labeled with plus signs and asterisks, respectively. The arrow at the bottom of the figure indicates the direction that peptide tilts away from the bilayer normal. (D) Schematic representation of the peptide helix at a 62° tilt angle with respect to the bilayer normal.

normal, on the time scale of the ^{2}H NMR experiments (less than $\sim 10^{-5}$ s).

The replacement of tryptophan with kynurenine alters not only the structure of SP-B_{8-25} but also its interactions with micelles, as revealed by the diffusion NMR studies. The translational diffusion measurements obtained from the 2D DOSY spectra demonstrate that the size and shape of SDS and DPC micelle complexes containing Kyn-SP-B_{8-25} are substantially different from those of the complexes containing Trp-SP-B_{8-25} (Figure 6 and Table 2). For each system, a total of three diffusion coefficients, and three corresponding apparent hydrodynamic diameters, are measured: two from the attenuation of the micelle peaks at 0.80 and 1.22 ppm and one from the peptide HN region (6−9 ppm). Taking the average, we find the apparent hydrodynamic diameters of the Trp-SP-B_{8-25}−SDS complex and Kyn-SP-B_{8-25}−SDS complex are 2.80 ± 0.05 and 3.72 ± 0.18 nm, respectively. On the other hand, the apparent hydrodynamic diameters of the Trp-SP-B_{8-25}−DPC complex and the Kyn-SP-B_{8-25}−DPC complex are 4.42 ± 0.16 and 3.77 ± 0.04 nm, respectively. Thus, in both micelle systems, a substantial change in the complex size (and/or shape) occurs, likely because of the altered micelle interactions of the oxidized peptide compared to those of the unmodified peptide. Interestingly, the changes in apparent hydrodynamic diameter for the zwitterionic versus anionic micelle systems are opposite.

Unrestrained MD simulations furthered our understanding of the effects on the peptide structure and interactions with lipids caused by tryptophan oxidation. MD simulations were run for 50 ns with Trp-SP-B_{8-28} and Kyn-SP-B_{8-25} in 7:3 DPPC/POPG monolayers. At the start of MD simulations, either the unmodified or the oxidized peptide was inserted 24 Å below the lipid headgroups, as measured from the top-most lipid atom to the bottom-most peptide atom, with a parallel orientation to the monolayer surface. All parameters examined appeared to be equilibrated by or before 40 ns, so the last 10 ns of each run was analyzed.

The snapshots taken at the end of the 50 ns simulations illustrate the difference in the positions of the peptides within monolayers (Figure 7). Both Trp-SP-B_{8-28} and Kyn-SP-B_{8-25} rise toward the aqueous phase from their initial depth to a similar final depth. However, the angle between the helical axis and the monolayer plane, as well as the disposition of the kynurenine and

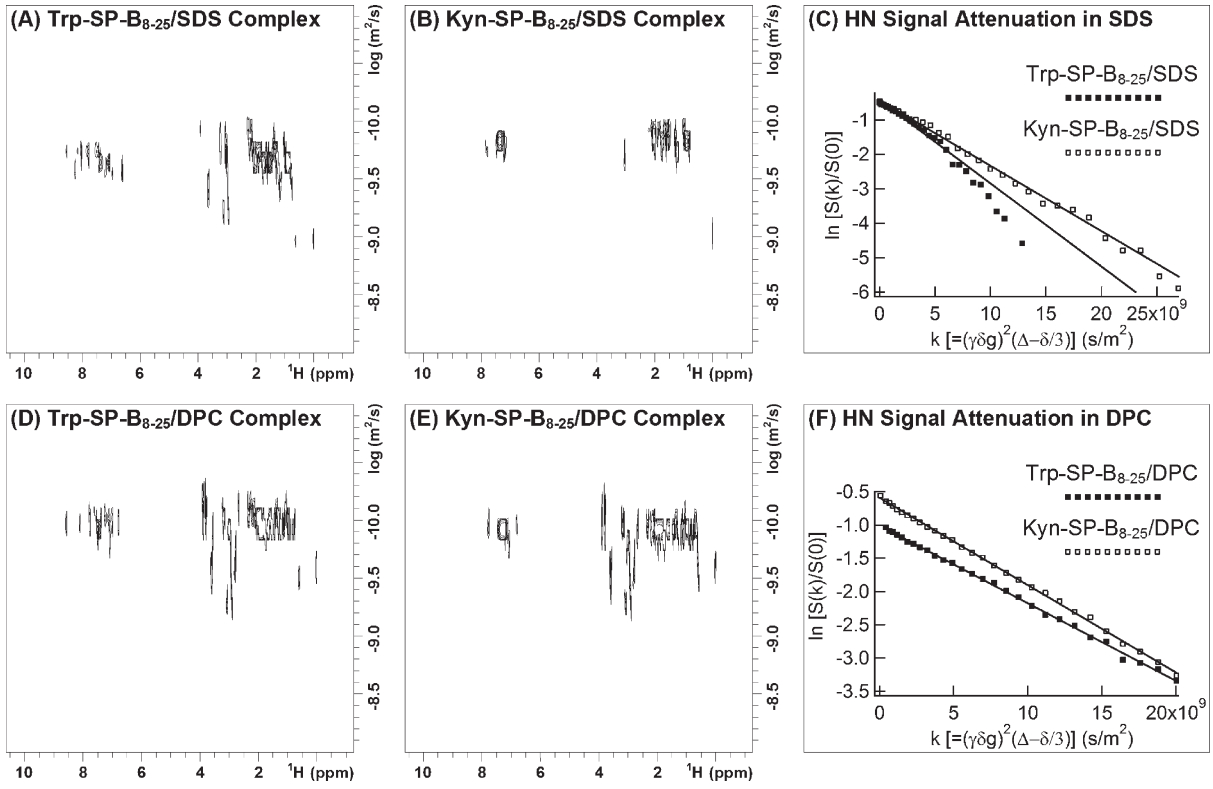

FIGURE 6: Translational diffusion measurements of SP-B_{8-25}−micelle complexes. Left panels show the 2D DOSY spectra of 1 mM Trp-SP-B_{8-25} in 100 mM SDS (A) and 100 mM DPC (D). Middle panels show the 2D DOSY spectra of 1 mM Kyn-SP-B_{8-25} in 100 mM SDS (B) and 100 mM DPC (E). Three values of translational diffusion coefficients, and corresponding hydrodynamic diameters, were calculated for each system using the slopes of the signal attenuation curves obtained from the micelle peaks at 0.80 and 1.22 ppm and the peptide HN region (6−9 ppm) (Table 2). The signal attenuation curves and fits for the HN regions are shown in the right panels (C and F).

Table 2: Observed Translational Diffusion Coefficients and Corresponding Apparent Hydrodynamic Diameters of SP-B_{8-25}−Micelle Complexes[a]

	observed diffusion coefficient ($\times 10^{-10}$ m^2/s)			apparent hydrodynamic diameter (nm)		
peptide−micelle complex composition	0.80 ppm	1.22 ppm	6−9 ppm	0.80 ppm	1.22 ppm	6−9 ppm
Trp-SP-B_{8-25}−SDS	2.33 ± 0.02	2.30 ± 0.01	2.42 ± 0.09	2.82	2.85	2.71
Kyn-SP-B_{8-25}−SDS	1.67 ± 0.02	1.74 ± 0.01	1.90 ± 0.04	3.93	3.77	3.45
Trp-SP-B_{8-25}−DPC	1.071 ± 0.003	1.087 ± 0.003	1.168 ± 0.009	4.57	4.51	4.19
Kyn-SP-B_{8-25}−DPC	1.278 ± 0.005	1.308 ± 0.003	1.312 ± 0.008	3.83	3.74	3.73

[a]For each system, three diffusion coefficients were determined from the DOSY spectra by fitting two micelle peaks (0.80 and 1.22 ppm) and the peptide HN region (6−9 ppm). The apparent diameters of the peptide−micelle complexes were calculated using the Stokes−Einstein equation.

neighboring side chains, appears to be quite different when compared to that of the tryptophan peptide. The tryptophan is positioned at the interface between the lipid headgroups and acyl chains, which is perfect for anchoring the peptide inside the lipid monolayer. By contrast, the position of kynurenine is much farther from the acyl chains and very close to the monolayer surface, where it can come in contact with the solvent water molecules.

Application of the DSSP algorithm (*45*) accurately assigns a secondary structure type to each residue, and quantification of the secondary structure over the last 10 ns of the MD runs clarifies the severity of the effects of tryptophan oxidation on the secondary structure of SP-B_{8-25} (Figure 8). For the unmodified peptide, Trp-SP-B_{8-25}, the structure remains largely α-helical over the full simulation period, except for the three to four C-terminal amino acids. However, with oxidation, i.e., replacement of tryptophan with kynurenine, the helical structure is substantially disrupted as only a few central residues of the peptide retain an α-helical conformation over the simulation period. The most prominent disruption is noticed at the N-terminus that contains the kynurenine. This loss of structure can be expected to relate to changes in how the peptide interacts with lipids.

The MD simulations also indicate that the peptide−lipid interactions are affected by the replacement of tryptophan with kynurenine. This is quantified in atom density plots calculated over the last 10 ns of the simulations, which show where the tryptophan and kynurenine residues of the corresponding peptides reside within the monolayers (Figure 9). For both systems, the region of highest lipid atom density is located at ~4.85 nm along the bilayer normal. The densest region of the phosphorus atoms, which indicates the position of the lipid headgroups, is at 5.35 nm and is similar for both systems. Interestingly, the region of highest tryptophan atom density for Trp-SP-B_{8-25} is at 4.75 nm along the bilayer normal, while that of kynurenine atoms from Kyn-SP-B_{8-25} is at 5.25 nm. Therefore, the kynurenine is

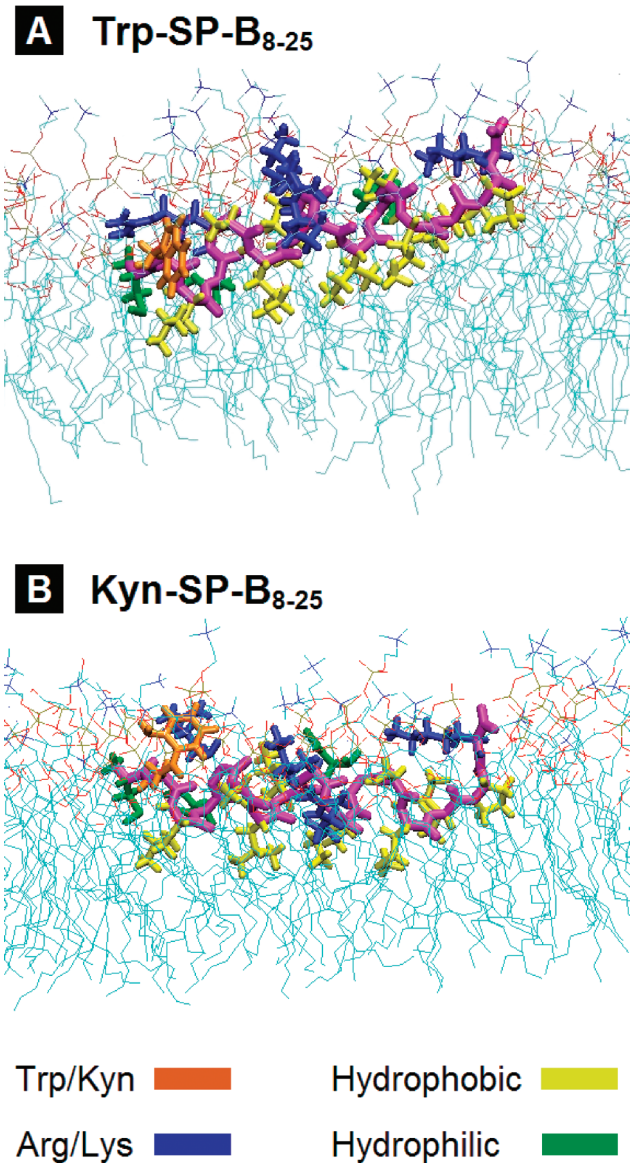

FIGURE 7: Snapshots from the molecular dynamics simulation of SP-B_{8-25} in DPPC/POPG (7:3) monolayers. Final positions of Trp-SP-B_{8-25} (A) and Kyn-SP-B_{8-25} (B) are shown at the end of 50 ns runs. The water layer is not shown in these snapshots for the sake of clarity.

positioned much closer to the phosphorus atoms, and hence to the aqueous phase above the monolayer surface, than is tryptophan in the corresponding peptide.

DISCUSSION

Inactivation of lung surfactant occurs in frequently fatal respiratory disorders like ARDS (*2*). There are multiple biophysical and biochemical alterations of lung surfactant associated with such conditions (*46*). However, several studies have indicated that patients with ARDS show clear evidence of increased oxidative damage to surfactant proteins as well as lipids (*14*−*19*). Oxidative modification of SP-B, an essential component of lung surfactant, appears to be a major contributor to surfactant inactivation (*8*, *15*, *19*). The modifications occur through a change in the chemical structures of the two methionines and of the single tryptophan present in the SP-B sequence (*21*). Oxidation of Trp9 is likely responsible for a large proportion of the deleterious effect as this amino acid is vital for SP-B

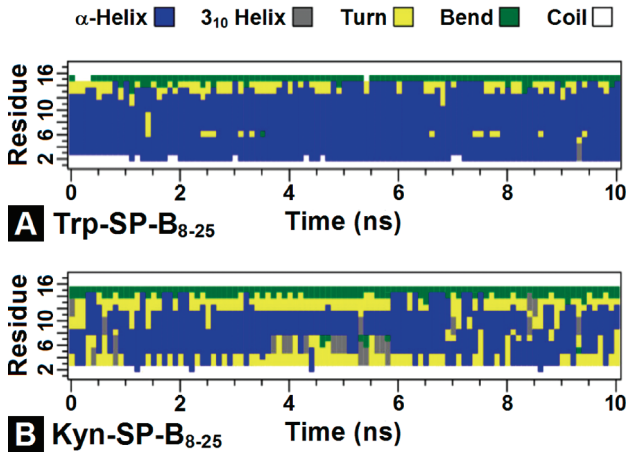

FIGURE 8: DSSP secondary structure assignment of Trp-SP-B_{8-25} (A) and Kyn-SP-B_{8-25} (B) vs simulation time over the last 10 ns of the molecular dynamics simulation.

function (*22*, *23*) and its oxidation appears to correlate with more severe effects on SP-B surface activity (*21*). Although the exact role of SP-B in lung surfactant function is still unknown, biophysical studies indicate that SP-B is involved in large-scale rearrangements of lipid structures required at various stages of the breathing cycle (*7*). Oxidation of tryptophan therefore has the potential to drastically affect SP-B's capability to reorganize the lipid structures.

SP-B_{8-25}, an 18-amino acid fragment comprising the N-terminal helical region of SP-B, is similar to other N-terminal SP-B peptides that have been shown to exhibit in vitro surface activity (*22*, *47*), as well as to retain partial biological function when included in artificial surfactants (*48*). Previous ^{2}H NMR studies of lipid bilayers containing SP-B_{8-25} suggested that this peptide interacts with lipids in such a way that the peptide interferes with the mixing of DPPC and POPG lipid components (*49*). SP-B_{8-25} carries a net charge of +4 at neutral pH as compared to the net charge of +7 for full-length SP-B. It also includes the only tryptophan present in the SP-B sequence. The function of SP-B is thought to relate to its positive charges and amphipathic helical structure (*50*, *51*), and thus, the retention of these structural features by the SP-B_{8-25} fragment presumably contributes to the partial functionality of this peptide. In this work, we have characterized the modifications to SP-B_{8-25} structure and lipid interactions caused by tryptophan oxidation using solution and solid-state NMR, along with circular dichroism and molecular dynamics simulations.

The structure of SP-B_{11-25} in methanol was studied by Kurtz et al. and found to be α-helical for amino acids 13−21 (*52*). However, this fragment did not include the functionally important Trp9. In another structural study, Mini-B, a larger peptide consisting of SP-B_{8-25} joined to SP-B_{63-78}, was found to consist of two α-helices. The N-terminal helix extended from residue 10 to 21 in SDS and from residue 11 to 22 in a 40% HFIP aqueous solution (*25*).

Solution NMR observations of Trp-SP-B_{8-25} indicate that the peptide adopts an α-helical conformation extending over 8−10 amino acids in both SDS and DPC micelles, as well as in HFIP (Figure 3). CD data also indicate that approximately half of the peptide is helical in all three environments (Figure 4 and Table 1). The rest of the peptide appears to be random and extended. The secondary structure of Trp-SP-B_{8-25} is thus not very different from that of the corresponding segment of Mini-B in either SDS

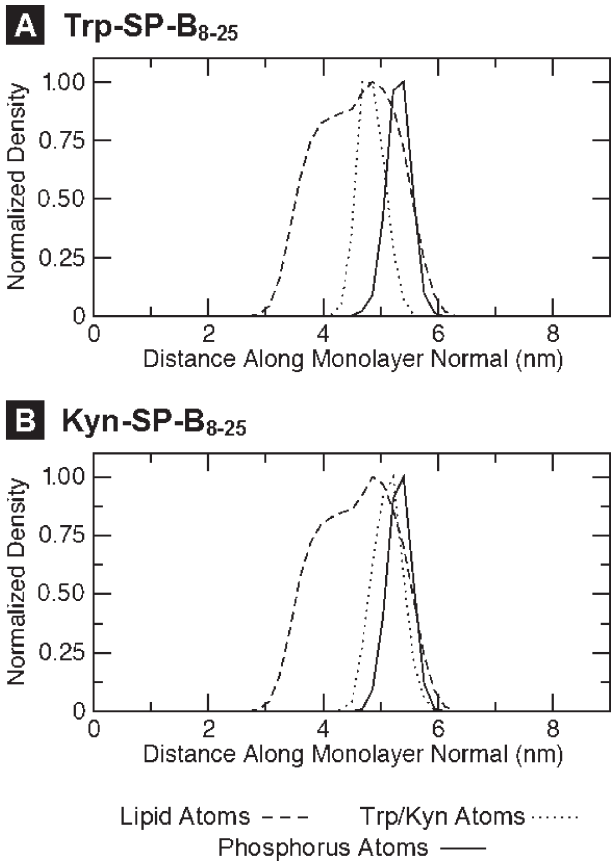

FIGURE 9: Atomic density plots showing the positions of tryptophan (A) and kynurenine (B) atoms with respect to the monolayer lipid and phosphorus atoms along the monolayer normal.

or HFIP. In these structures, the N-terminal helix extends over 12 amino acids. It is therefore reasonable to assume that, despite the slight shortening of the helix, the Trp-SP-B_{8-25} backbone structure alone is similar to that within Mini-B in which the three positively charged amino acids (Arg12, Lys16, and Arg17) cluster on one face and the four nonpolar amino acids (Leu10, Leu14, Ile15, and Ile18) cluster on the opposite face. Consideration of the Mini-B structure suggests that Trp9 is unlikely to be a part of the helix but rather is located just before the N-terminal end of the helix. The Mini-B structure also suggests that the tryptophan is positioned near the interface between the charged and hydrophobic faces of the peptide. This positioning is conducive to the tryptophan side chain interacting with both polar and apolar moieties in the lipids to anchor the peptide at the lipid−water interface. Tryptophan likely contributes to SP-B function in two linked ways: by providing lipid anchoring that helps facilitate SP-B's role in rearranging lipid structures and by contributing to the overall amphipathicity of the helix that is important to the stabilization of its structure in the presence of a lipid interface. Disruptions in the amphipathic profile of the peptide could thus lead to inactivation both by direct effects on lipid interactions and indirectly by decreasing the stability of the structure as a whole.

Solid-state ^{2}H NMR data reveal the orientation and dynamics of Trp-SP-B_{8-25} in a POPC bilayer environment (Figure 5). The spectra indicate that the peptide undergoes rapid reorientation about the bilayer normal with a characteristic reorientation correlation time on the order of $< 10^{-5}$ s. Interestingly, the peptide displays an orientation with its helix long axis tilted by ~60° away from the bilayer normal; i.e., although it is an amphipathic peptide, it is tilted ~30° away from a purely in-plane position. In membrane proteins, tryptophan, arginine, and lysine residues all have roles in anchoring membrane proteins to the polar−apolar interface. Their positions with respect to the bilayer interface are, however, typically different. For example, tryptophan tends to occupy a well-defined site in the lipid carbonyl region, while lysine is positioned closer to the aqueous phase (*53*). It would thus appear likely that the balance between the side chain−lipid interactions of the Trp, Arg, Lys, and other residues of Trp-SP-B_{8-25} holds it in a somewhat tilted position in the bilayer. This oblique positioning of the peptide has been proposed to be critical to the activity of other amphipathic peptides such as fusogenic peptides (e.g., ref *54*) that like SP-B (*7*) function by modifying lipid bilayer structure. The tilt angle of Kyn-SP-B_{8-25} could not be measured experimentally using the same alanine-deuterated approach applied to Trp-SP-B_{8-25} because of the loss of helical structure. However, in the MD simulations, Trp-SP-B_{8-25} was observed to be positioned at an angle in the monolayer with the tryptophan end of the helix positioned relatively deeply, while Kyn-SP-B_{8-25} was oriented parallel to the interface (Figure 7).

As shown by the solution NMR data (Figures 2 and 3) and the CD data (Figure 4 and Table 1), the α-helical structure of SP-B_{8-25} is drastically disrupted when tryptophan is replaced with one of its oxidized forms, kynurenine. The helical stretch of approximately three turns is reduced to one turn, at most, in both SDS and DPC micelles, as well as in 40% HFIP. The loss of structure in SDS and DPC micelles is consistent with a role for tryptophan amphipathicity in stabilizing the helical structure of the peptide in the context of a polar−apolar interface. That the loss was greater in SDS than DPC (25% for SDS vs 18% for DPC) implies that interactions with negatively charged lipid headgroups are important for promoting overall helix stability. The loss of structure in HFIP needs to be interpreted differently because this solvent system stabilizes structure by mechanisms different from those of micelles, in particular by stabilizing hydrogen bonds (*55*, *56*). However, the loss of structure induced by tryptophan oxidation does appear to be somewhat generic, as it was observed in all three environments.

The diffusion NMR data (Figure 6) provide evidence of altered peptide−lipid interactions as a result of replacement of tryptophan with kynurenine in SP-B_{8-25}, at least in the context of highly curved detergent micelles. The DOSY-derived observed translational diffusion coefficient is converted into apparent hydrodynamic diameter, i.e., the diameter of a sphere apparently diffusing at the same rate, using the Stokes−Einstein equation (Table 2). The diffusion coefficients reflect a variety of parameters related to peptide−micelle interactions, including the size of the complex and the ratio of free to bound species (*57*), and to a lesser extent the shape of the complex (*58*), and crowding effects (*59*). The apparent hydrodynamic diameter of the Kyn-SP-B_{8-25}−SDS complex is substantially larger (3.7 nm) than that of the Trp-SP-B_{8-25}−SDS complex (2.8 nm), reflecting oxidation-induced changes in the peptide's interactions with micelles. The structure of Trp-SP-B_{8-25}, with an intact cationic, amphipathic helix, is suitable for strong interaction with both negatively charged headgroups and hydrophobic acyl chains of the SDS micelle. These interactions apparently lead to a relatively compact complex of the peptide and the micelle. However, when the tryptophan is replaced with kynurenine, a large portion of the helix becomes unstructured. This likely disrupts the clustering of

the positive charges and causes them to spread over a larger area on the peptide surface, affecting the interactions between the peptide and the micelle. The consequent loosening of the binding to SDS, and perhaps stretching of the SDS micelle to accommodate the unstructured Kyn-SP-B_{8-25}, are consistent with the increased apparent hydrodynamic diameter of the Kyn-SP-B_{8-25}−SDS complex compared to that of the Trp-SP-B_{8-25}−SDS complex.

That SP-B is more effective in reducing surface tension when PG, rather than unsaturated PC, is present with DPPC in model surfactants (*60*, *61*) is one indication that interactions with negatively charged headgroups are an important part of SP-B's function. This issue was probed by repeating the translational diffusion measurements with zwitterionic DPC micelles, in place of anionic SDS micelles. Indeed, the diffusion NMR data of SP-B_{8-25} in DPC micelles represent a somewhat different behavior when compared to those in SDS micelles. The difference between the apparent hydrodynamic diameters of the Trp-SP-B_{8-25}- and Kyn-SP-B_{8-25}-containing micelles is not as large for DPC as it is in SDS micelles and is opposite; i.e., the apparent hydrodynamic diameter of the Kyn-SP-B_{8-25}−DPC complex is smaller (3.8 nm) than that of the Trp-SP-B_{8-25}−DPC complex (4.4 nm). There are several plausible scenarios that may contribute to this observation. As DPC headgroups contain both positive and negative charges, the electrostatic component of the peptide−micelle interactions may not be as strong in DPC as in SDS. As a result, Trp-SP-B_{8-25} is probably not as compactly bound to the DPC micelle as to the SDS micelle. Thus, when tryptophan is replaced with kynurenine, the helix is disrupted; however, the overall electrostatic and hydrophobic interactions between the peptide and the DPC micelle may not change much, and hence, the apparent hydrodynamic diameters of the complexes may not be drastically different. Also, the position of Trp-SP-B_{8-25} in the DPC micelle may not be as deep as it is in the SDS micelle, again because of the difference in the electrostatic part of the peptide−micelle interactions. Therefore, disruption in the SP-B_{8-25} helix resulting from the Trp to Kyn substitution may not produce a substantial change in the surface area of the DPC micelle because the peptide positioning is relatively shallow. This hypothesis is favorably supported by the observation that SP-B_{63-78}, the C-terminal half of Mini-B with a degree of amphipathicity similar to that of SP-B_{8-25} (due to three clustered positive charges), takes a deeper position inside anionic phospholipid-containing bilayers (mimicked by SDS in this study) than in purely zwitterionic bilayers (mimicked by DPC in this study) (*27*). Lastly, because of the loss of amphiphilicity, Kyn-SP-B_{8-25} may not be able to bind as many DPC molecules in the complex as Trp-SP-B_{8-25} can. Hence, the apparent hydrodynamic diameter of the micelle complex containing the oxidized peptide may be smaller than that of the complex containing the unmodified peptide.

We have also performed unrestrained molecular dynamics simulations for both Trp-SP-B_{8-25} and Kyn-SP-B_{8-25} in DPPC/POPG monolayers to gain additional insight into the mechanistic details that underlie the effects of tryptophan oxidation on the peptide's structure and lipid interactions. Monolayers were chosen for these simulations rather than bilayers, as monolayers at the air−water interface are key in lung surfactant function (*62*), and because the results could be compared to those for similar monolayers simulated in the absence of peptide (*39*). Results of the simulations displayed through DSSP (Figure 8) show a distinct loss of the α-helical structure in SP-B_{8-25} because of the replacement of tryptophan with kynurenine. This loss is consistent with the experimental data and involves unwinding of the helix at both the N- and C-termini, but more prominently at the N-terminus. Snapshots from MD simulations (Figure 7) show that the overall orientation of Kyn-SP-B_{8-25} is different from that of Trp-SP-B_{8-25}, with Trp-SP-B_{8-25} in a more tilted position, in agreement with the ^{2}H NMR observations, and Kyn-SP-B_{8-25} more parallel to the monolayer surface. Most striking is the difference between the positions of tryptophan and kynurenine side chains. Tryptophan positions itself at the lipid interface with the hydrophobic aromatic ring facing toward the lipid acyl chains. In contrast, kynurenine is positioned farther from the lipid acyl chains and much closer to the aqueous phase. Atomic density plots (Figure 9), averaged over the last 10 ns of the simulations, further emphasize that kynurenine is positioned much closer to the phosphorus atoms of the lipid headgroups and the water layer than tryptophan. Therefore, oxidation appears to alter the orientation of SP-B_{8-25} within the monolayer.

The changes in the structure and lipid interaction of SP-B_{8-25} upon oxidation presumably stem from the differing chemical and electronic properties of tryptophan and kynurenine. Upon oxidation, the polar five-member ring of tryptophan containing the imino group is disrupted. While the tryptophan side chain possesses only a single hydrogen bond donor site, the kynurenine side chain contains three donor/acceptor sites. It is therefore possible that the kynurenine side chain competes with the peptide backbone in forming non-native hydrogen bonds. This seems the most likely explanation for the loss of structure in HFIP. Probably more relevant for the loss of structure observed in the micelle systems is the fact that oxidation decreases the hydrophobicity of the tryptophan side chain, altering the amphipathic profile of the peptide surface and thus decreasing its stabilization by the micelle. There are other factors potentially affecting the oxidized peptide structure. For example, cation−π interactions between arginine and tryptophan can be important for peptide structure and function (*63*) and would be absent in the kynurenine version of the peptide. As revealed by the high-resolution structure of Mini-B (*25*), the side chains of Trp9 and Arg12 (Trp2 and Arg5, respectively, in Mini-B) are oriented almost parallel to each other. Loss of this interaction may contribute to unfolding of the Kyn-SP-B_{8-25} helix from this end.

Oxidative modification of SP-B, particularly the tryptophan residue, is a major source of lung surfactant dysfunction in conditions like ARDS (*8*, *15*, *19*, *21*). This study reveals that the impact of tryptophan oxidation on the helical structure and lipid interactions of the N-terminal helix of SP-B is indeed severe. It is likely that these effects are interlinked, with disruption of the lipid interactions of oxidized SP-B_{8-25} leading to a reduction in the level of helix stabilization provided by the micelle/bilayer environment, while disruption of the structure leads to modifications of the lipid interactions that are important to the function of the peptide. The ^{2}H NMR studies revealed that unmodified SP-B_{8-25} is oriented with its helical axis tilted ~30° from the bilayer plane, and the diffusion data indicate severe disruptions to the peptide−micelle interactions upon oxidation. Additionally, the MD simulations, combined with what is known about the preferred depth of tryptophan, indicate that oxidation of the peptide is very likely to lead to the helix being positioned more parallel to the bilayer plane. Interestingly, in the context of the many studies addressing the lipid binding preferences of SP-B (*64*−*66*), the diffusion data also indicate that the characteristics of the disruptions to the peptide−lipid interactions caused by oxidation are

very dependent on the lipid headgroup, with opposite effects observed for anionic micelles versus zwitterionic micelles.

Conducting these studies with a small SP-B construct comprising the N-terminal helical region of SP-B was essential for allowing the consequences of tryptophan oxidation to be revealed in detail but obviously introduced some uncertainty into how the results should be extended to full-length SP-B. In particular, it is expected that residues 1−7 of full-length SP-B impact its lipid interactions. These residues are highly hydrophobic and thus are thought to insert deeply into phospholipid bilayers. Inclusion of these residues has been shown to improve the surfactant properties of Mini-B and enhance peptide dimerization in SDS micelles (*67*). Also, SP-B_{1-25} causes the formation of fluid isotropic lipid phases, and the presence of residues 1−7 alters the effects of the N-terminus of SP-B on lipid dynamics (*68*). While residues 1−7 were excluded from this study to allow the characterization of the effect of tryptophan oxidation on the N-terminal helix of SP-B, uncomplicated by the presence of this insertion sequence and, in particular, its tendency to promote dimerization, the next stage of the work will include the insertion sequence. That said, given the known functional consequences of full-length SP-B oxidation (*8*, *15*, *19*, *21*) and that SP-B N-terminal helix peptides retain part of the function of the full-length protein (*22*, *47*, *48*, *69*, *70*), we expect that comparable oxidation-induced disruptions to protein structure and lipid interactions occur in the context of full-length SP-B.

ACKNOWLEDGMENT

The high-performance computing facilities employed in the MD simulations were provided by ACEnet (Atlantic Canadian Computational Excellence network). We are particularly grateful to Dr. Mansour Almaterneh for performing the Gaussian calculations with kynurenine and to Dr. Michael Hayley and Dr. David Heeley for help with the circular dichroism studies.

REFERENCES

1. Hallman, M., Glumoff, V., and Ramet, M. (2001) Surfactant in respiratory distress syndrome and lung injury. *Comp. Biochem. Physiol., Part A: Mol. Integr. Physiol. 129*, 287–294.
2. Seeger, W., Gunther, A., Walmrath, H. D., Grimminger, F., and Lasch, H. G. (1993) Alveolar surfactant and adult respiratory distress syndrome: Pathogenetic role and therapeutic prospects. *Clin. Invest. 71*, 177–190.
3. Melton, K. R., Nesslein, L. L., Ikegami, M., Tichelaar, J. W., Clark, J. C., Whitsett, J. A., and Weaver, T. E. (2003) SP-B deficiency causes respiratory failure in adult mice. *Am. J. Physiol. 285*, L543–L549.
4. Nogee, L. M., Garnier, G., Dietz, H. C., Singer, L., Murphy, A. M., deMello, D. E., and Colten, H. R. (1994) A mutation in the surfactant protein B gene responsible for fatal neonatal respiratory disease in multiple kindred's. *J. Clin. Invest. 93*, 1860–1863.
5. Clark, J. C., Wert, S. E., Bachurski, C. J., Stahlman, M. T., Stripp, B. R., Weaver, T. E., and Whitsett, J. A. (1995) Targeted disruption of the surfactant protein B gene disrupts surfactant homeostasis, causing respiratory failure in newborn mice. *Proc. Natl. Acad. Sci. U.S.A. 92*, 7794–7798.
6. Robertson, B., Kobayashi, T., Ganzuka, M., Grossmann, G., Li, W. Z., and Suzuki, Y. (1991) Experimental neonatal respiratory failure induced by a monoclonal antibody to the hydrophobic surfactant-associated protein SP-B. *Pediatr. Res. 30*, 239–243.
7. Hawgood, S., Derrick, M., and Poulain, F. (1998) Structure and properties of surfactant protein B. *Biochim. Biophys. Acta 1408*, 150–160.
8. Rodriguez-Capote, K., Faulkner, J., Possmayer, F., and Nag, K. (2005) Alteration of alveolar surfactant function by reactive oxygen species. In Lung Surfactant Function and Disorder (Nag, K., and Lenfant, C., Eds.) pp 425−448, Taylor & Francis Group, Boca Raton, FL.
9. Haagsman, H. P. (1998) Oxidative damage of the pulmonary surfactant system. *Semin. Neonatol. 3*, 207–217.
10. Gunther, A., Ruppert, C., Schmidt, R., Markart, P., Grimminger, F., Walmrath, D., and Seeger, W. (2001) Surfactant alteration and replacement in acute respiratory distress syndrome. *Respir. Res. 2*, 353–364.
11. Lewis, J. F., and Veldhuizen, R. (2003) The role of exogenous surfactant in the treatment of acute lung injury. *Annu. Rev. Physiol. 65*, 613–642.
12. Putman, E., van Golde, L. M., and Haagsman, H. P. (1997) Toxic oxidant species and their impact on the pulmonary surfactant system. *Lung 175*, 75–103.
13. Seeger, W., Lepper, H., Wolf, H. R., and Neuhof, H. (1985) Alteration of alveolar surfactant function after exposure to oxidative stress and to oxygenated and native arachidonic acid in vitro. *Biochim. Biophys. Acta 835*, 58–67.
14. Andersson, S., Kheiter, A., and Merritt, T. A. (1999) Oxidative inactivation of surfactants. *Lung 177*, 179–189.
15. Gilliard, N., Heldt, G. P., Loredo, J., Gasser, H., Redl, H., Merritt, T. A., and Spragg, R. G. (1994) Exposure of the hydrophobic components of porcine lung surfactant to oxidant stress alters surface tension properties. *J. Clin. Invest. 93*, 2608–2615.
16. Mark, L., and Ingenito, E. P. (1999) Surfactant function and composition after free radical exposure generated by transition metals. *Am. J. Physiol. 276*, L491–L500.
17. Haddad, I. Y., Zhu, S., Ischiropoulos, H., and Matalon, S. (1996) Nitration of surfactant protein A results in decreased ability to aggregate lipids. *Am. J. Physiol. 270*, L281–L288.
18. Ingbar, D. H., Bair, R., Jung, P., Heinecke, J., and Haddad, I. Y. (1999) Hyperoxic lung injury increases HOCl-modified lung proteins and Na,K-adenosine triphosphatase nitrotyrosine content. *Chest 116* (Suppl. 1), 100S.
19. Rodriguez-Capote, K., Manzanares, D., Haines, T., and Possmayer, F. (2006) Reactive oxygen species inactivation of surfactant involves structural and functional alterations to surfactant proteins SP-B and SP-C. *Biophys. J. 90*, 2808–2821.
20. Bridges, J. P., Davis, H. W., Damodarasamy, M., Kuroki, Y., Howles, G., Hui, D. Y., and McCormack, F. X. (2000) Pulmonary surfactant proteins A and D are potent endogenous inhibitors of lipid peroxidation and oxidative cellular injury. *J. Biol. Chem. 275*, 38848–38855.
21. Manzanares, D., Rodriguez-Capote, K., Liu, S., Haines, T., Ramos, Y., Zhao, L., Doherty-Kirby, A., Lajoie, G., and Possmayer, F. (2007) Modification of tryptophan and methionine residues is implicated in the oxidative inactivation of surfactant protein B. *Biochemistry 46*, 5604–5615.
22. Ryan, M. A., Qi, X., Serrano, A. G., Ikegami, M., Perez-Gil, J., Johansson, J., and Weaver, T. E. (2005) Mapping and analysis of the lytic and fusogenic domains of surfactant protein B. *Biochemistry 44*, 861–872.
23. Serrano, A., Ryan, M., Weaver, T., and Perez-Gil, J. (2006) Critical Structure-Function Determinants within the N-Terminal Region of Pulmonary Surfactant Protein SP-B. *Biophys. J. 90*, 238–249.
24. Yau, W. M., Wimley, W. C., Gawrisch, K., and White, S. H. (1998) The preference of tryptophan for membrane interfaces. *Biochemistry 37*, 14713–14718.
25. Sarker, M., Waring, A. J., Walther, F. J., Keough, K. M. W., and Booth, V. (2007) Structure of Mini-B, a Functional Fragment of Surfactant Protein B, in Detergent Micelles. *Biochemistry 46*, 11047–11056.
26. Waring, A. J., Walther, F. J., Gordon, L. M., Hernandez-Juviel, J. M., Hong, T., Sherman, M. A., Alonso, C., Alig, T., Braun, A., Bacon, D., and Zasadzinski, J. A. (2005) The role of charged amphipathic helices in the structure and function of surfactant protein B. *J. Pept. Res. 66*, 364–374.
27. Yang, T., McDonald, M., Morrow, M. R., and Booth, V. (2009) The effect of a C-terminal peptide of surfactant protein B (SP-B) on oriented lipid bilayers, characterized by solid-state ^{2}H- and ^{31}P-NMR. *Biophys. J. 96* (9), 3762–3771.
28. Liu, M., Mao, X. A., Ye, C., Huang, H., Nicholson, J. K., and Lindon, J. C. (1998) Improved WATERGATE pulse sequences for solvent suppression in NMR spectroscopy. *J. Magn. Reson. 132*, 125–129.
29. Morris, K. F., and Johnson, C. S. (1992) Diffusion-ordered two dimensional nuclear magnetic resonance spectroscopy. *J. Am. Chem. Soc. 114* (8), 3139–3141.
30. Tanner, J. E. (1970) Use of the stimulated echo in NMR diffusion studies. *J. Chem. Phys. 52*, 2523–2526.
31. Sklenar, V., Piotto, M., Leppik, R., and Saudek, V. (1993) Gradient-tailored water suppression for proton-nitrogen-15 HSQC experiments optimized to retain full sensitivity. *J. Magn. Reson. 102*, 241–245.
32. Davis, J., Jeffrey, K., Bloom, M., Valic, M., and Higgs, T. (1976) Quadrupole echo deuteron magnetic resonance spectroscopy in ordered hydrocarbon chains. *Chem. Phys. Lett. 42*, 390–394.

33. Davis, J. (1983) The description of membrane lipid conformation, order and dynamics by ^{2}H-NMR. *Biochim. Biophys. Acta 737*, 117–171.
34. Jones, D., Barber, K., van der Loo, E., and Grant, C. (1998) Epidermal growth factor receptor transmembrane domain: ^{2}H NMR implications for orientation and motion in a bilayer environment. *Biochemistry 37*, 16780–16787.
35. van der Wel, P., Strandberg, E., Killian, J., and Koeppe, R. (2002) Geometry and intrinsic tilt of a tryptophan-anchored transmembrane α-helix etermined by ^{2}H NMR. *Biophys. J. 83* (3), 1479–1488.
36. Heeley, D. H., and Hong, C. (1994) Isolation and characterization of tropomyosin from fish muscle. *Comp. Biochem. Physiol. 108* (1), 95–106.
37. Yang, J. T., Wu, C. S., and Martinez, H. M. (1989) Calculation of protein conformation from circular dichroism. *Methods Enzymol. 130*, 208–269.
38. Lindahl, E., Hess, B., and van der Spoel, D. (2001) Gromacs 3.0: A package for molecular simulation and trajectory analysis. *J. Mol. Model. 7*, 306–317.
39. Rose, D., Rendell, J., Lee, D., Nag, K., and Booth, V. (2008) Molecular dynamics simulations of lung surfactant lipid monolayers. *Biophys. Chem. 138*, 67–77.
40. Frisch, M. J., Trucks, G. W., Schlegel, H. B., Scuseria, G. E., Robb, M. A., Cheeseman, J. R., Scalmani, G., Barone, V., Mennucci, B., Petersson, G. A., Nakatsuji, H., Caricato, M., Li, X., Hratchian, H. P., Izmaylov, A. F., Bloino, J., Zheng, G., Sonnenberg, J. L., Hada, M., Ehara, M., Toyota, K., Fukuda, R., Hasegawa, J., Ishida, M., Nakajima, T., Honda, Y., Kitao, O., Nakai, H., Vreven, T., Montgomery, J. A., Jr., Peralta, J. E., Ogliaro, F., Bearpark, M., Heyd, J. J., Brothers, E., Kudin, K. N., Staroverov, V. N., Kobayashi, R., Normand, J., Raghavachari, K., Rendell, A., Burant, J. C., Iyengar, S. S., Tomasi, J., Cossi, M., Rega, N., Millam, N. J., Klene, M., Knox, J. E., Cross, J. B., Bakken, V., Adamo, C., Jaramillo, J., Gomperts, R., Stratmann, R. E., Yazyev, O., Austin, A. J., Cammi, R., Pomelli, C., Ochterski, J. W., Martin, R. L., Morokuma, K., Zakrzewski, V. G., Voth, G. A., Salvador, P., Dannenberg, J. J., Dapprich, S., Daniels, A. D., Farkas, O., Foresman, J. B., Ortiz, J. V., Cioslowski, J., and Fox, D. J. (2009) Gaussian 09, revision A.1, Gaussian, Inc., Wallingford, CT.
41. Jorgensen, W. L., Maxwell, D. S., and Tirado-Rives, J. (1996) Development and testing of the OPLS all-atom force field on conformational energetics and properties of organic liquids. *J. Am. Chem. Soc. 118*, 11225–11236.
42. Tieleman, D. P., MacCallum, J. L., Ash, W. L., Kandt, C., Xu, Z., and Monticelli, L. (2006) Membrane protein simulations with a united-atom lipid and all-atom protein model: Lipid-protein interactions, side chain transfer free energies and model proteins. *J. Phys.: Condens. Matter 18* (28), S1221–S1234.
43. Wuthrich, K. (1986) NMR of Proteins and Nucleic Acids, John Wiley & Sons, New York.
44. Strandberg, E., Esteban-Martin, S., Salgado, J., and Ulrich, A. (2009) Orientation and dynamics of peptides in membranes calculated from ^{2}H-NMR data. *Biophys. J. 96*, 3223–3232.
45. Kabsch, W., and Sander, C. (1983) Dictionary of protein secondary structure: Pattern recognition of hydrogen-bonded and geometrical features. *Biopolymers 22* (12), 2577–2637.
46. Hartog, A., Gommers, D., and Lachmann, B. (1995) Role of surfactant in the pathophysiology of the acute respiratory distress syndrome (ARDS). *Monaldi Arch. Chest Dis. 50*, 372–377.
47. Veldhuizen, E. J., Waring, A. J., Walther, F. J., Batenburg, J. J., van Golde, L. M., and Haagsman, H. P. (2000) Dimeric N-terminal segment of human surfactant protein B (dSP-B(1−25)) has enhanced surface properties compared to monomeric SP-B(1−25). *Biophys. J. 79*, 377–384.
48. Revak, S. D., Merritt, T. A., Hallman, M., Heldt, G., La Polla, R. J., Hoey, K., Houghten, R. A., and Cochrane, C. G. (1991) The use of synthetic peptides in the formation of biophysically and biologically active pulmonary surfactants. *Pediatr. Res. 29*, 460–465.
49. Russell-Schulz, B., Booth, V., and Morrow, M. R. (2009) Perturbation of DPPC/POPG bilayers by the N-terminal helix of lung surfactant protein SP-B: A ^{2}H NMR study. *Eur. Biophys. J. 38* (5), 613–624.
50. Longo, M. L., Bisagno, A. M., Zasadzinski, J. A., Bruni, R., and Waring, A. J. (1993) A function of lung surfactant protein SP-B. *Science 261*, 453–456.
51. Baatz, J. E., Sarin, V., Absolom, D. R., Baxter, C., and Whitsett, J. A. (1991) Effects of surfactant-associated protein SP-B synthetic analogs on the structure and surface activity of model membrane bilayers. *Chem. Phys. Lipids 60*, 163–178.
52. Kurutz, J. W., and Lee, K. Y. C. (2002) NMR structure of lung surfactant peptide SP-B_{11-25}. *Biochemistry 41*, 9627–9636.
53. de Planque, M. R. R., Kruijtzer, J. A. W., Liskamp, R. M. J., Marsh, D., Greathouse, D. V., Koeppe, R. E., II, de Kruijff, B., and Killian, J. A. (1999) Different Membrane Anchoring Positions of Tryptophan and Lysine in Synthetic Transmembrane α-Helical Peptides. *J. Biol. Chem. 274*, 20839–20846.
54. Kirat, K. E., Lins, L., Brasseur, R., and Dufrene, Y. F. (2005) Fusogenic tilted peptides induce nanoscale holes in supported phosphatidylcholine bilayers. *Langmuir 21*, 3116–3121.
55. Roccatano, D., Fioroni, M., Zacharias, M., and Colombo, G. (2005) Effect of hexafluoroisopropanol alcohol on the structure of melittin: A molecular dynamics simulation study. *Protein Sci. 14*, 2582–2589.
56. Yoshida, K., Yamaguchi, T., Adachi, T., Otomo, T., Matsuo, D., Takamuku, T., and Nishi, N. (2003) Structure and dynamics of hexafluoroisopropanol-water mixtures by X-ray diffraction, small-angle neutron scattering, NMR spectroscopy, and mass spectrometry. *J. Chem. Phys. 119*, 6132–6142.
57. Göbl, C., Dulle, M., Hohlweg, W., Grossauer, J., Falsone, S. F., Glatter, O., and Zangger, K. (2010) Influence of phosphocholine alkyl chain length on peptide-micelle interactions and micellar size and shape. *J. Phys. Chem. B 114*, 4717–4724.
58. Marshall, A. G. (1978) Biophysical Chemistry: Principles, Techniques and Applications, John Wiley & Sons, New York.
59. Barhoum, S., and Yethiraj, A. (2009) An NMR study of macromolecular aggregation in a model polymer-surfactant solution. *J. Chem. Phys. 132*, 024909.
60. Rodriguez-Capote, K., Nag, K., Schürch, S., and Possmayer, F. (2001) Surfactant protein interactions with neutral and acidic phospholipid films. *Am. J. Physiol. 281*, L231–L242.
61. Ingenito, E. P., Mora, R., and Mark, L. (2000) Pivotal role of anionic phospholipids in determining dynamic behavior of lung surfactant. *Am. J. Respir. Crit. Care Med. 161* (3), 831–838.
62. Schurch, S., Qanbar, R., Bachofen, H., and Possmayer, F. (1995) The surface-associated surfactant reservoir in the alveolar lining. *Biol. Neonate 67* (Suppl. 1), 61–76.
63. Chan, D. I., Prenner, E. J., and Vogel, H. J. (2006) Tryptophan- and arginine-rich antimicrobial peptides: Structures and mechanisms of action. *Biochim. Biophys. Acta 1758*, 1184–1202.
64. Baatz, J. E., Elledge, B., and Whitsett, J. A. (1990) Surfactant protein SP-B induces ordering at the surface of model membrane bilayers. *Biochemistry 29*, 6714–6720.
65. Perez-Gil, J., Casals, C., and Marsh, D. (1995) Interactions of hydrophobic lung surfactant proteins SP-B and SP-C with dipalmitoylphosphatidylcholine and dipalmitoylphosphatidylglycerol bilayers studied by electron spin resonance spectroscopy. *Biochemistry 34*, 3964–3971.
66. Breitenstein, D., Batenburg, J. J., Hagenhoff, B., and Galla, H. J. (2006) Lipid specificity of surfactant protein B studied by time-of-flight secondary ion mass spectrometry. *Biophys. J. 91* (4), 1347–1356.
67. Walther, F. J., Waring, A. J., Hernandez-Juviel, J. M., Gordon, L. M., Wang, Z., Jung, C., Ruchala, P., Clark, A. P., Smith, W. M., Sharma, S., and Notter, R. H. (2010) Critical structural and functional roles for the N-terminal insertion sequence in surfactant protein B analogs. *PLoS One 5* (1), e8672.
68. Farver, R. S., Mills, F. D., Antharam, V. C., Chebukati, J. N., Fanucci, G. E., and Long, J. R. (2010) Lipid polymorphism induced by surfactant peptide SP-B1-25. *Biophys. J. 99* (6), 1773–1782.
69. Tanaka, Y., Takei, T., Aiba, T., Masuda, K., Kiuchi, A., and Fujiwara, T. (1986) Development of synthetic lung surfactants. *J. Lipid Res. 27*, 475–485.
70. Walther, F. J., Hernandez-Juviel, J. M., Gordon, L. M., Sherman, M. A., and Waring, A. J. (2002) Dimeric surfactant protein B peptide SP-B 1−25 in neonatal and acute respiratory distress syndrome. *Exp. Lung Res. 28*, 623–640.